Society of Medical Education & Research

2024, Volume 4, Issue 2, Page No: 96-121
ISSN: 3108-4834

Archive of International Journal of Cancer and Allied Science

Degradation of Oncogenic DDX3X by KLHL29-CUL3 Ubiquitin Ligase Abrogates Cell Cycle Progression and Overcomes Chemoresistance in Triple-Negative Breast Cancer

Viktor Andras Horvath[1]*, Balazs Peter Nemeth[1], Katalin Eva Kiss[1]

[1]Department of Oncology, Semmelweis University, Budapest, Hungary.

***E-mail** ✉ v.horvath.semmelweis@gmail.com

Abstract

Triple-negative breast cancer (TNBC) is a diverse subtype of breast cancer, constituting about 15–20% of all breast cancer cases. This study highlights KLHL29, an under-researched gene within the Kelch-like gene family, as an important tumor suppressor that influences chemoresistance in TNBC. Compared to adjacent normal tissues, KLHL29 expression was significantly reduced in breast cancer tissues, and lower levels of KLHL29 correlated with poor prognosis. Overexpression of KLHL29 inhibited, while its depletion promoted, the growth, migration, and invasion of TNBC cells. Mechanistically, KLHL29 interacted with the CUL3 E3 ligase, targeting the RNA-binding protein DDX3X for degradation via the proteasome. This degradation led to the destabilization of CCND1 mRNA, causing cell cycle arrest in the G0/G1 phase. Notably, combining the DDX3X inhibitor RK33 with platinum-based chemotherapy enhanced the suppression of TNBC, particularly in models with low KLHL29 and high DDX3X expression. These findings suggest that the KLHL29-DDX3X pathway plays a crucial role in TNBC progression and presents a promising strategy to overcome chemoresistance.

Keywords: Breast cancer, Chemoresistance, Tumor, Chemotherapy

Introduction

Breast cancer remains the most prevalent malignancy and a leading cause of cancer-related death in women worldwide [1]. Triple-negative breast cancer (TNBC) accounts for roughly 15–20% of breast cancer diagnoses, characterized by the lack of estrogen receptors, progesterone receptors, and human epidermal growth factor receptor 2 (HER2) [2-4]. TNBC is biologically diverse, often exhibiting larger tumor sizes, higher grades, and greater metastatic potential [5, 6]. Due to the absence of targetable receptors, patients with TNBC do not benefit from traditional hormonal or HER2-targeted therapies [7]. Recently, novel therapies such as immunotherapy, targeted treatments, and antibody-drug conjugates have emerged, reshaping TNBC treatment [8]. However, standard cytotoxic chemotherapy, based on anthracyclines and taxanes, remains the cornerstone of treatment, though many patients eventually develop resistance [9, 10]. Given the aggressive nature of TNBC and the absence of effective treatments and biomarkers, understanding the mechanisms behind TNBC progression and chemoresistance is an ongoing research focus.

In previous work, we explored the genomic, transcriptomic, and proteomic landscape of TNBC in Chinese patients from Fudan University Shanghai Cancer Center (FUSCC), offering critical molecular insights for further clinical research [11, 12]. From this, we identified key genes driving TNBC progression, such as PDSS1, which facilitates metastasis through the CAMK2A-STAT3 pathway [13], and ENSA, which enhances cholesterol biosynthesis via STAT3 and SREBP2 signaling [14]. Another gene, MARCO, contributes to metabolic dysregulation and hypoxic

Access this article online https://smerpub.com/

Received: 09 May 2024; **Accepted:** 14 September 2024

How to cite this article: Horvath VA, Nemeth BP, Kissn KE. Degradation of Oncogenic DDX3X by KLHL29-CUL3 Ubiquitin Ligase Abrogates Cell Cycle Progression and Overcomes Chemoresistance in Triple-Negative Breast Cancer. Arch Int J Cancer Allied Sci. 2024;4(2):96-121. https://doi.org/10.51847/OUiP5C98Ml

tumor conditions by modulating HIF-1α signaling [15]. These findings highlight the molecular mechanisms driving TNBC, but in this study, we focus on identifying tumor suppressors, particularly KLHL29, an underexplored member of the Kelch-like gene family.

The KLHL gene family encodes evolutionarily conserved proteins, typically featuring a BTB/POZ domain, a BACK domain, and multiple Kelch motifs [16]. These proteins are involved in several cellular processes, including mitosis, DNA repair, autophagy, and apoptosis, primarily through their interaction with the E3 ubiquitin ligase CUL3 [17, 18]. Some KLHL proteins are known to play crucial roles in tumorigenesis and cancer progression [19-22]. In this study, we show that KLHL29 acts as a tumor suppressor in TNBC. Its expression is significantly lower in cancerous compared to normal tissues, and reduced KLHL29 levels correlate with poor patient prognosis. Overexpressing KLHL29 suppressed TNBC cell proliferation and metastasis, while its depletion accelerated disease progression. KLHL29 regulates the ubiquitination and degradation of the RNA-binding protein DDX3X via CUL3, which leads to cell cycle arrest at G0/G1. Combining platinum-based chemotherapy with the DDX3X inhibitor RK33 showed promising results in treating TNBC, particularly in tumors with low KLHL29 and high DDX3X expression. This study uncovers the tumor-suppressive function of KLHL29 in TNBC and presents a potential strategy for overcoming chemoresistance.

Materials and Methods

Clinical specimens and datasets

Triple-negative breast cancer (TNBC) samples were collected from patients undergoing surgical procedures at the Breast Surgery Department of the First Hospital of China Medical University, all of whom had not received prior therapy. Diagnoses were confirmed by expert pathologists, and complete follow-up records were available. All procedures followed the principles of the Declaration of Helsinki and were approved by the Institutional Ethics Review Board of the First Hospital of China Medical University. Written informed consent was obtained from all participants. In addition, publicly available datasets, including the FUSCC-TNBC cohort, TCGA, and CPTAC, were analyzed to complement the study.

Mouse xenograft studies

Female NOD/SCID and BALB/c-nude mice aged 4–6 weeks were sourced from the Department of Laboratory Animal Science, Shanghai Medical College of Fudan University. To evaluate KLHL29 overexpression, 1 × 10^6 MDA-MB-231 cells expressing KLHL29 or a control vector (pCDH-CMV-MCS-EF1-puro) were mixed with 100 μL of PBS:Matrigel (1:1) and orthotopically implanted into the mammary fat pads of NOD/SCID mice. For KLHL29 knockdown experiments, 1 × 10^6 MDA-MB-231 cells stably expressing shNC or sh-KLHL29 were injected similarly. The effects of combining RK33 with cisplatin or carboplatin were tested in BALB/c-nude mice implanted with MDA-MB-231 cells and divided into four treatment groups: vehicle, RK33, platinum drugs, or the combination. RK33 (20 mg/kg), cisplatin (3 mg/kg), or carboplatin (15 mg/kg) in 200 μL was administered intraperitoneally three times per week. All injections were performed with the investigator blinded to group allocation. Tumor growth was measured using electronic calipers in two dimensions, and tumor volumes were calculated as: volume = length × width × width × 0.52. Mice were euthanized at study endpoints, and tumors were collected for downstream analysis. All procedures were approved by the Animal Welfare Committee of Shanghai Medical College, Fudan University.

Organoid culture

Patient-derived organoids (PDOs) were generated from freshly resected TNBC tissues following established protocols [23]. Tumor samples were minced into 1–3 mm^3 pieces and enzymatically digested with collagenase and hyaluronidase on an orbital shaker for 1–2 h at 37 °C. The resulting suspension was filtered through a 100 μm mesh, centrifuged at 1500 rpm for 5 min, and incubated in 10 mL TAC buffer for 3 min to remove red blood cells. After further washing and centrifugation, cell clusters were embedded in type-2 Basement Membrane Extract (BME, Trevigen, 3533-010-02) as 40 μL droplets on pre-warmed 24-well plates and polymerized at 37 °C for 20 min. Organoids were maintained in breast cancer organoid medium under a humidified atmosphere of 5% CO2 at 37 °C. Following 3–5 passages, organoids were seeded into 384-well plates and cultured for 5 days before drug exposure. Drug-treated organoids were incubated for 1 week, and viability was assessed using the CellTiter-Glo 3D Cell viability assay (Promega, #G9683). Images were captured on the final day to observe morphological changes.

Statistical analysis

All analyses were conducted using GraphPad Prism (v9.4.1), R (v4.0.3), and SPSS (v26.0). Comparisons between two groups were performed with Wilcoxon rank-sum tests, two-tailed Student's t tests, or two-way ANOVA as appropriate. Spearman correlation was used for correlation analyses. Kaplan-Meier survival curves were plotted and compared using log-rank tests. Multivariate Cox proportional hazard models were applied to compute hazard ratios with 95% confidence intervals. Data are presented as mean ± SD from at least three independent experiments. $P < 0.05$ was considered statistically significant (*p < 0.05; **p < 0.01; ***p < 0.001; ns, not significant).

Results and Discussion

Reduced KLHL29 expression associates with poor outcomes in triple-negative breast cancer

Using multi-omics profiling from the FUSCC TNBC cohort [11], we identified KLHL29, a member of the KLHL family that has not been extensively studied, as significantly underexpressed in TNBC tissues compared to adjacent normal breast tissues **(Figure 1a).** This trend persisted across 88 paired samples, showing consistent downregulation **(Figure 1b).** Analysis of TNBC datasets from TCGA further confirmed that KLHL29 mRNA levels are lower in tumors versus normal tissues (**Figures 1c and 1d).**

Protein-level validation was performed on six pairs of primary TNBC and matched non-tumor tissues by western blotting. To determine the clinical significance, we performed survival analyses. Kaplan–Meier plots indicated that patients with basal-like breast cancer exhibiting low KLHL29 expression had significantly shorter overall survival and relapse-free survival, based on the Kaplan–Meier plotter database **(Figures 1e–1h).** Additionally, IHC staining of KLHL29 was performed in 91 surgical TNBC samples collected at the First Hospital of China Medical University **(Figure 1i).** Tumors with weak KLHL29 expression showed worse overall survival **(Figure 1j)** and relapse-free survival **(Figure 1k).** Multivariate Cox regression confirmed that low KLHL29 levels serve as an independent predictor of poor prognosis in TNBC patients.

Overall, these data highlight that KLHL29 is markedly reduced in TNBC at both the mRNA and protein levels, and its downregulation is strongly associated with unfavorable clinical outcomes.

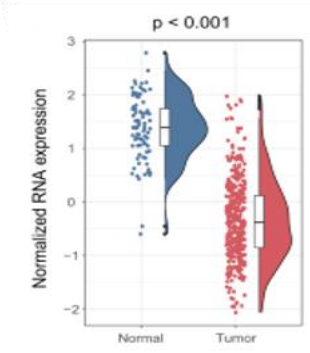

a)

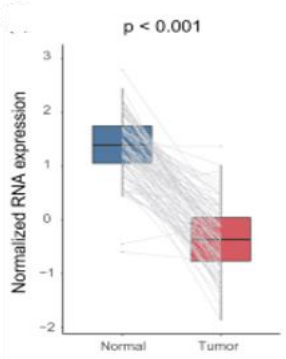

b)

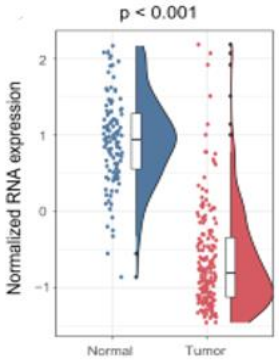

c)

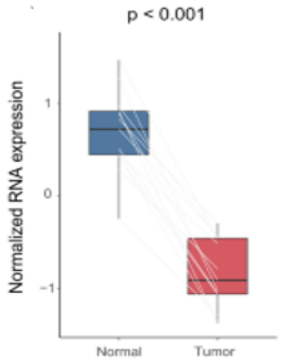
p < 0.001
Normalized RNA expression
1
0
−1
Normal
Tumor

d)

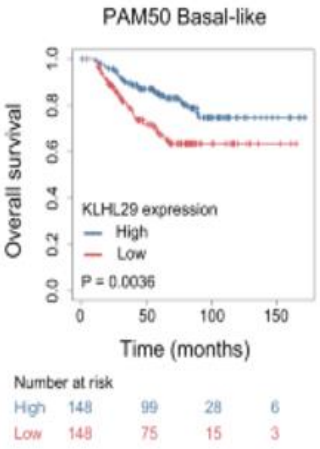
PAM50 Basal-like
Overall survival
0.0
0.2
0.4
0.6
0.8
1.0
KLHL29 expression
High
Low
P = 0.0036
0
50
100
150
Time (months)
Number at risk
High 148 99 28 6
Low 148 75 15 3

e)

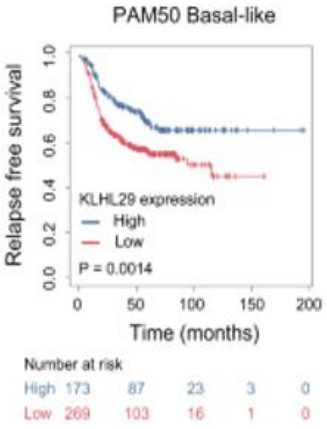
PAM50 Basal-like
Relapse free survival
0.0
0.2
0.4
0.6
0.8
1.0
KLHL29 expression
High
Low
P = 0.0014
0
50
100
150
200
Time (months)
Number at risk
High 173 87 23 3 0
Low 269 103 16 1 0

f)

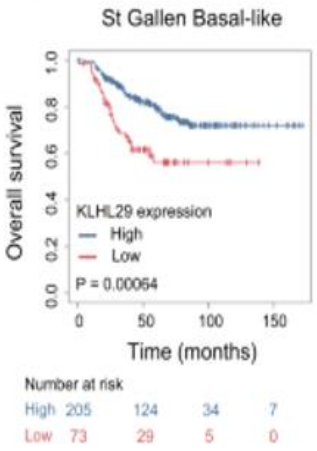
St Gallen Basal-like
Overall survival
0.0
0.2
0.4
0.6
0.8
1.0
KLHL29 expression
High
Low
P = 0.00064
0
50
100
150
Time (months)
Number at risk
High 205 124 34 7
Low 73 29 5 0

g)

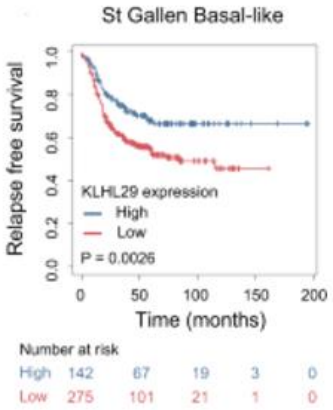
St Gallen Basal-like
Relapse free survival
0.0
0.2
0.4
0.6
0.8
1.0
KLHL29 expression
High
Low
P = 0.0026
0
50
100
150
200
Time (months)
Number at risk
High 142 67 19 3 0
Low 275 101 21 1 0

h)

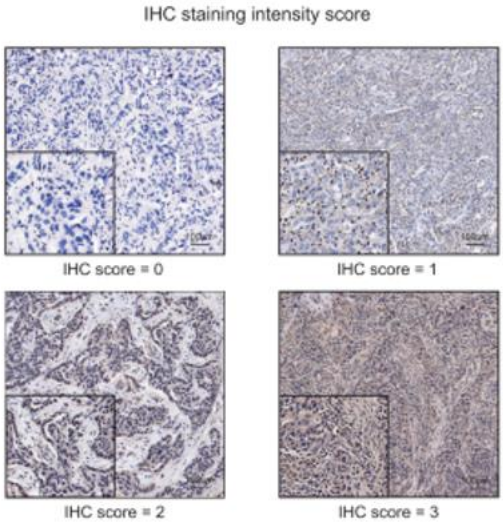
IHC staining intensity score
IHC score = 0
IHC score = 1
IHC score = 2
IHC score = 3

i)

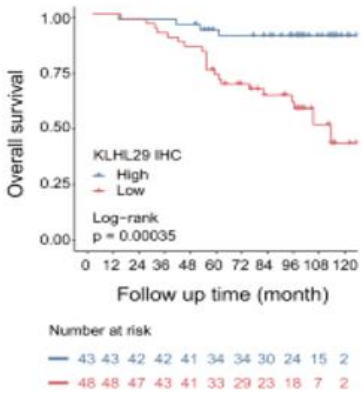

j)

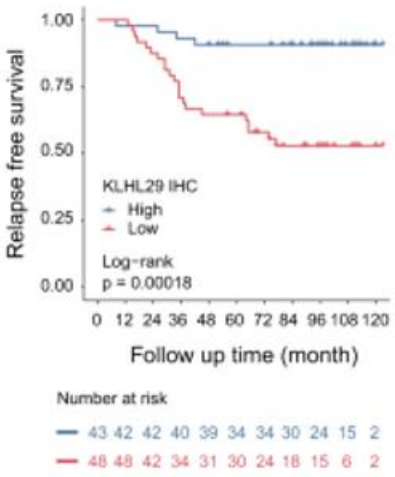

k)

Figure 1. KLHL29 expression is reduced in TNBC, and its decreased expression correlates with poorer outcomes.

(a) mRNA levels of KLHL29 in 360 TNBC samples and 88 adjacent normal tissues from the FUSCC-TNBC RNA-seq dataset.

(b) mRNA levels of KLHL29 in 88 TNBC samples and corresponding normal breast tissues from the FUSCC-TNBC RNA-seq dataset.

(c) mRNA levels of KLHL29 in 169 TNBC samples and 113 adjacent normal tissues from the TCGA TNBC RNA-seq dataset.

(d) mRNA levels of KLHL29 in 13 TNBC samples and paired normal tissues from the TCGA TNBC RNA-seq dataset. Data presented as mean ± SD. Statistical analysis was performed using the Wilcoxon rank-sum test.

(e–h) Kaplan–Meier survival curves for KLHL29 in basal-like breast cancer across PAM50 and St Gallen subtypes (https://kmplot.com/analysis/), analyzed using log-rank tests.

(i) Immunohistochemical analysis of KLHL29 expression in TNBC tissues with representative images provided.

(j, k) Reduced KLHL29 expression is associated with poorer overall survival (j) and relapse-free survival (k) based on log-rank test results.

KLHL29 inhibits cell growth, migration, and invasion in TNBC.

To explore KLHL29's role in TNBC, we first measured its protein levels in several established TNBC cell lines (BT549, CAL51, SUM159PT, MDA-MB-231, LM2-4175, Hs578T, HCC1806) and HEK293T cells using Western blotting **(Figure 2a).** We then introduced KLHL29 overexpression into BT549 and CAL51 cells via lentiviral vectors, as these cell lines express low baseline levels of KLHL29. The successful overexpression of KLHL29 was confirmed by Western blot and qRT-PCR **(Figures 2b and 2c).** Viability assays demonstrated that ectopic KLHL29 expression significantly inhibited TNBC cell proliferation **(Figures 2d and 2e)**. Colony formation assays indicated that KLHL29 overexpression reduced the colony-forming capacity of TNBC cells **(Figures 2f and 2c).** Flow cytometry analysis showed that KLHL29 overexpression led to increased apoptosis in TNBC cells **(Figures 2h and 2i).** Given the metastatic potential of TNBC, we also tested KLHL29's impact on migration and invasion. Transwell assays revealed that KLHL29 overexpression impaired the migration and invasion abilities of TNBC cells **(Figures 2j–m).** Additionally, we overexpressed KLHL29 in the highly aggressive MDA-MB-231 cell line. As with BT549 and CAL51 cells, KLHL29 overexpression suppressed cell proliferation in MDA-MB-231 cells. We performed xenograft studies using MDA-MB-231 cells with or without KLHL29 overexpression. Tumor growth was significantly reduced in the KLHL29-overexpressing group, as assessed by tumor size **(Figure 2n)**, growth rate **(Figure 2o)**, and weight **(Figure 2p)**. Immunohistochemical analysis showed reduced Ki67 staining in KLHL29-overexpressing tumors compared to controls. These results confirm that KLHL29 acts as a tumor suppressor and inhibits TNBC progression.

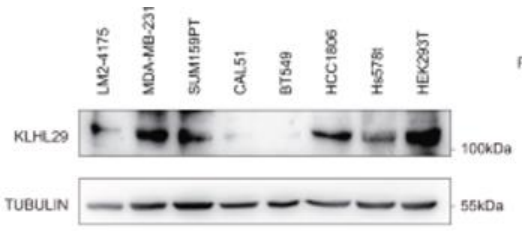
LM2-4175
MDA-MB-231
SUM159PT
CAL51
BT549
HCC1806
Hs578t
HEK293T
KLHL29
100kDa
TUBULIN
55kDa

a)

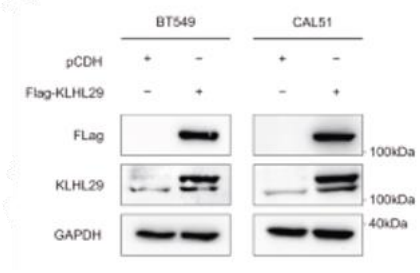
BT549
CAL51
pCDH
Flag-KLHL29
FLag
KLHL29
GAPDH
100kDa
100kDa
40kDa

b)

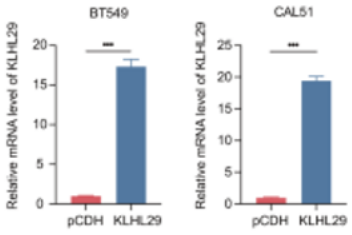
BT549
CAL51
Relative mRNA level of KLHL29
pCDH
KLHL29

c)

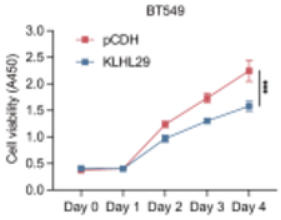
BT549
pCDH
KLHL29
Cell viability (A450)
Day 0 Day 1 Day 2 Day 3 Day 4

d)

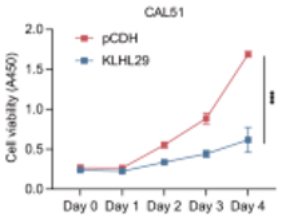
CAL51
pCDH
KLHL29
Cell viability (A450)
Day 0 Day 1 Day 2 Day 3 Day 4

e)

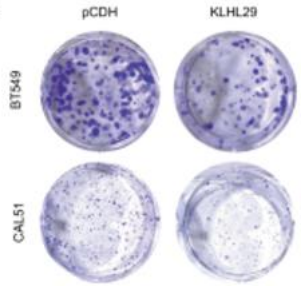
pCDH
KLHL29
BT549
CAL51

f)

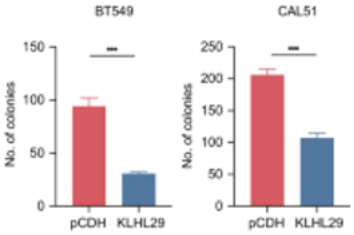
BT549
CAL51
No. of colonies
pCDH
KLHL29

g)

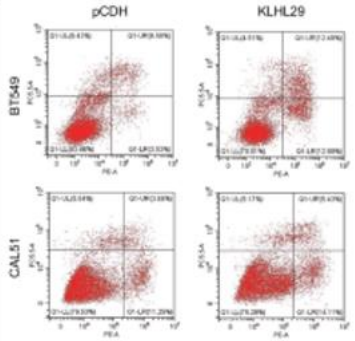
pCDH
KLHL29
BT549
CAL51

h)

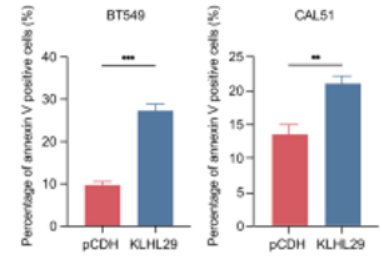
BT549
CAL51
Percentage of annexin V positive cells (%)
pCDH
KLHL29

i)

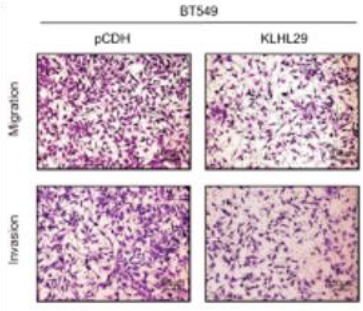
BT549
pCDH
KLHL29
Migration
Invasion

j)

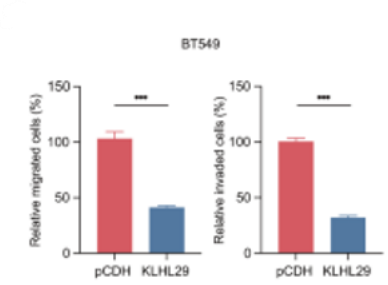

k)

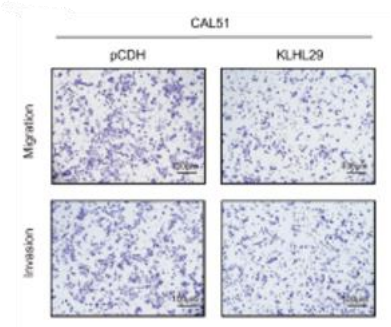

l)

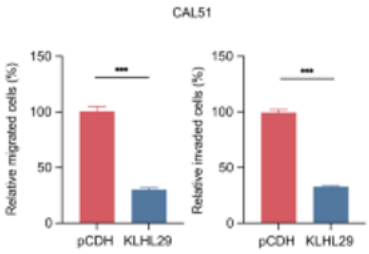

m)

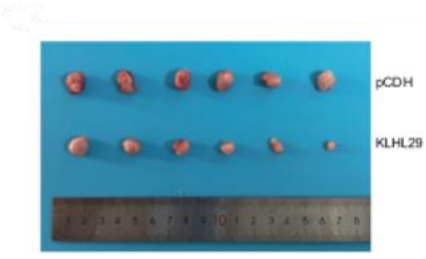

n)

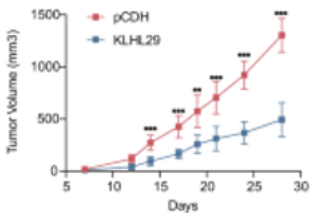

o)

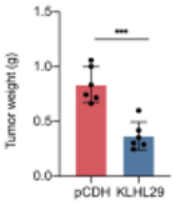

p)

Figure 2. KLHL29 restrains TNBC cell growth, migration, and invasion**.**

(a) Western blot analysis of KLHL29 protein levels in TNBC cell lines and HEK293T cells.

(b, c) KLHL29 expression was validated in BT549 and CAL51 cells stably transfected with either pCDH-Flag or pCDH-Flag-KLHL29, confirmed by Western blot (b) and RT-qPCR (c).

(d, e) Cell proliferation assays (Cell Counting Kit-8) showed that KLHL29 overexpression in BT549 (d) and CAL51 (e) cells led to reduced cell growth.

(f, g) Colony formation assays revealed that overexpressing KLHL29 decreased the colony-forming capability of both BT549 and CAL51 cells. Representative colony images (f) and corresponding quantitative data (g) are shown.

(h, i) Flow cytometry results indicated that KLHL29 overexpression increased apoptosis in BT549 and CAL51 cells, with images of cell apoptosis (h) and annexin V-positive cell percentages (i) shown.

(j–m) Transwell assays revealed that KLHL29 overexpression diminished migration and invasion of BT549 and CAL51 cells. Images of migrated and invaded cells (j, l) and quantitative results (K, M) are provided.

(n–p) In vivo experiments with MDA-MB-231 cells overexpressing KLHL29 demonstrated reduced tumor growth in xenograft models. Tumors were injected into NOD/SCID female nude mice (n = 6 per group), with representative images (n), tumor growth rates (o), and weights (p) presented. $^{**}p < 0.01$; $^{***}p < 0.001$ by two-tailed Student's t-test or two-way ANOVA.

KLHL29 depletion accelerates TNBC cell growth, migration, and invasion

Next, we examined the effects of reducing KLHL29 expression by silencing it with two distinct siRNAs in MDA-MB-231 and SUM159PT cells **(Figures 3a–3d).** KLHL29 knockdown significantly enhanced both cell proliferation **(Figures 3e and 3f)** and colony formation **(Figures 3g and 3h)** while reducing apoptosis **(Figures**

3i and 3j) in both cell types. Moreover, KLHL29 depletion increased the migratory and invasive capabilities of these cells **(Figures 3k–3n).** Stable knockdown of KLHL29 also stimulated growth in MDA-MB-231 cells and reintroducing KLHL29 into these cells reversed the effects on proliferation and migration. In xenograft models, depletion of KLHL29 resulted in significantly larger tumors, with increased tumor size **(Figure 3o)**, growth rate **(Figure 3p)**, and weight **(Figure 3q).** Immunohistochemical analysis indicated enhanced Ki67 staining in KLHL29-depleted tumors compared to controls. These results confirm that the loss of KLHL29 promotes TNBC progression.

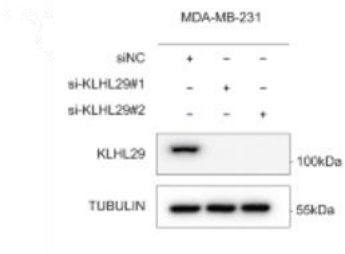

a)

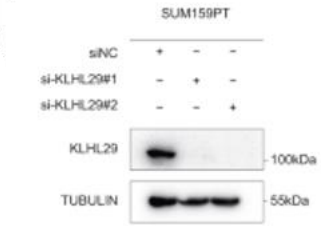

b)

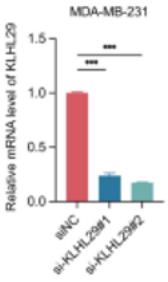

c)

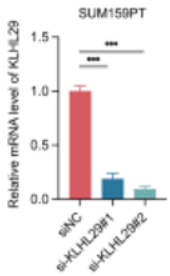

d)

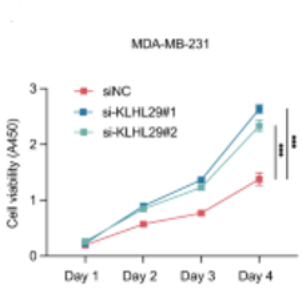

e)

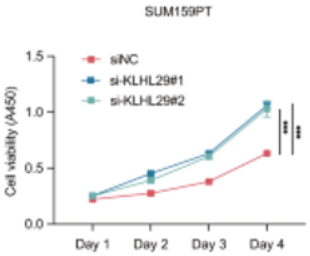

f)

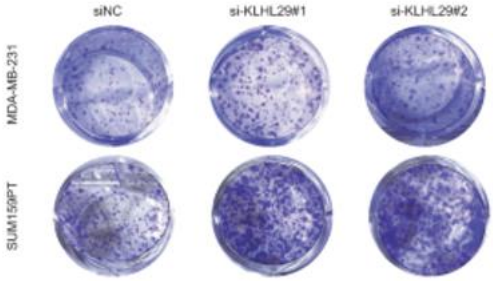

g)

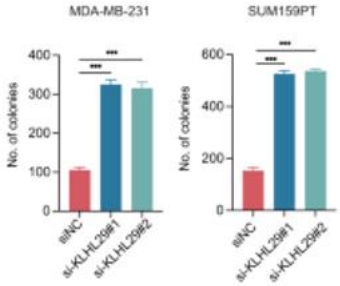

h)

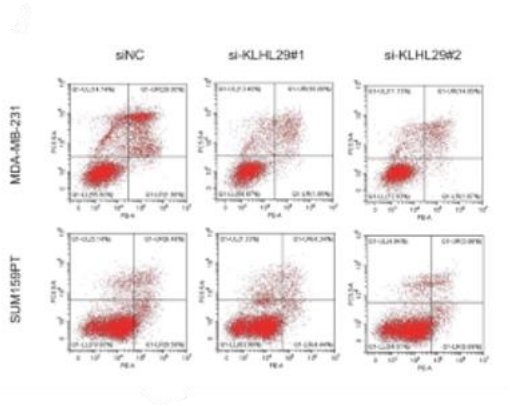

i)

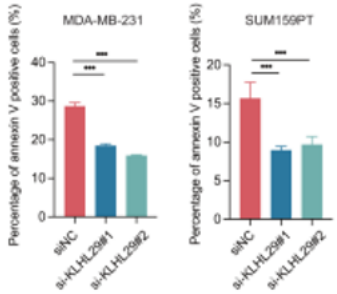

j)

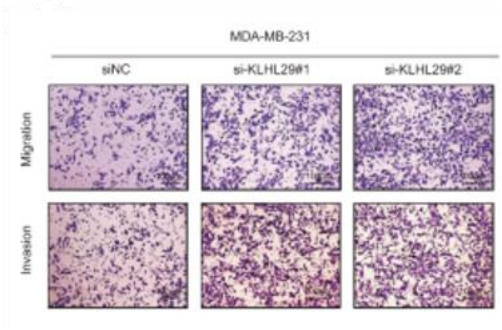

k)

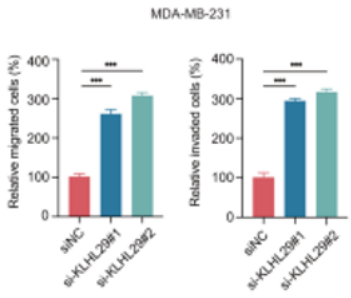

l)

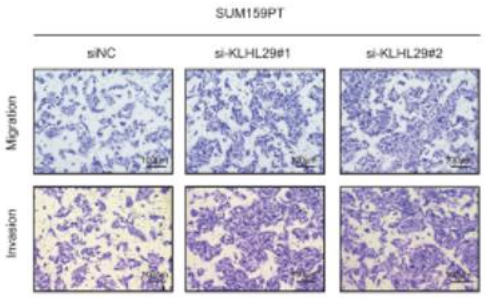

m)

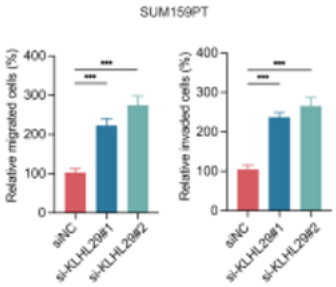

n)

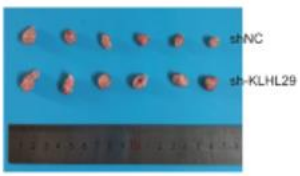

o)

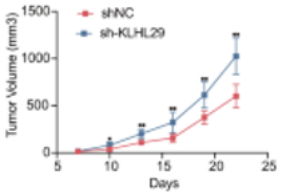

p)

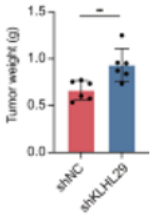

q)

Figure 3. Reduction of KLHL29 enhances proliferative, migratory, and invasive behaviors in TNBC cells. (a, b) Western blotting confirmed effective suppression of KLHL29 protein in MDA-MB-231 (a) and

SUM159PT (b) cells following transfection with two independent KLHL29-targeting siRNAs.
(c, d) RT-qPCR analysis further validated the decrease in KLHL29 transcript levels in MDA-MB-231 (c) and SUM159PT (d) cells upon siRNA-mediated silencing.
(E, F) Cell Counting Kit-8 assays demonstrated that loss of KLHL29 markedly increased proliferative capacity in MDA-MB-231 (e) and SUM159PT (f) cells.
(g, h) Clonogenic assays revealed a substantial rise in colony formation after KLHL29 knockdown in both cell models. Representative colony images (g) and statistical quantification (h) are shown.
(i, j) Flow cytometric evaluation indicated a reduction in apoptotic cell populations following KLHL29 depletion. Representative apoptosis profiles (i) and proportions of annexin V–positive cells (j) are presented.
(k–n) Transwell-based assays showed that silencing KLHL29 significantly elevated migration and invasion in MDA-MB-231 and SUM159PT cells, using uncoated or Matrigel-coated chambers, respectively. Representative microscopic images (k, m) and quantitative analyses (l, n) are provided.
(o–q) In vivo experiments demonstrated that KLHL29 loss accelerates xenograft tumor development. MDA-MB-231 cells stably expressing shNC or shKLHL29 were orthotopically implanted into the mammary fat pads of NOD/SCID female nude mice (n = 6 per group). Representative tumors (o), tumor growth kinetics (P), and excised tumor weights (q) are shown. **p < 0.01; ***p < 0.001 by two-tailed Student's t test or two-way ANOVA.

KLHL29 directly associates with DDX3X and suppresses its abundance

To uncover the molecular mechanism responsible for KLHL29-mediated tumor inhibition in TNBC, immunoprecipitation combined with mass spectrometry (IP–MS) was employed to identify proteins interacting with KLHL29 in BT549 and CAL51 cells **(Figure 4a).** This approach identified 46 candidate binding proteins in BT549 cells and 69 in CAL51 cells associated with Flag-tagged KLHL29 **(Figure 4b).** Among these candidates, the RNA helicase DDX3X—a protein with established oncogenic relevance—was consistently detected in both cell types **(Figure 4c).**

Proteomic data from the FUSCC-TNBC cohort showed that DDX3X protein levels were elevated in tumor tissues compared with matched non-tumorous samples [12]. Analysis of the CPTAC dataset further confirmed that DDX3X expression was significantly higher in TNBC and basal-like breast cancer relative to other molecular subgroups. Immunohistochemical evaluation demonstrated that patients exhibiting increased DDX3X expression experienced inferior clinical outcomes compared with those displaying lower expression levels. Multivariate Cox regression analysis identified elevated DDX3X as an independent predictor of poor survival in TNBC patients.

Functionally, RNA interference–mediated depletion of DDX3X significantly impaired TNBC cell proliferation and markedly reduced migratory and invasive capabilities. These findings support an oncogenic role for DDX3X and suggest that KLHL29 exerts its tumor-suppressive effects, at least partially, through negative regulation of DDX3X, a mechanism explored in subsequent experiments.

a)

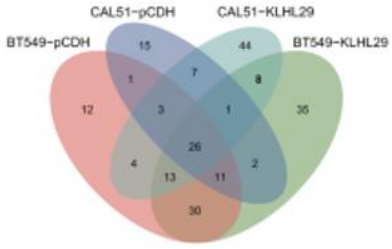

b)

Accession	Proteins	BT549 Unique Peptides	CAL51 Unique Peptides
Q96CT2	KLHL29	30	24
P62266	RPS23	2	1
Q92598	HSPH1	2	1
O00571	**DDX3X**	2	1
P01834	IGKC	1	1
P46781	RPS9	1	1
Q2PPJ7	RALGAPA2	1	1
P23381	WARS1	1	2

c)

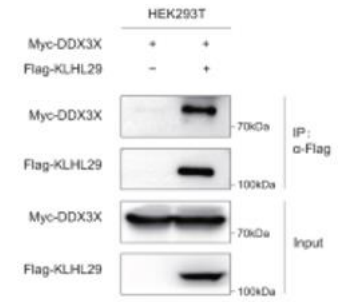

d)

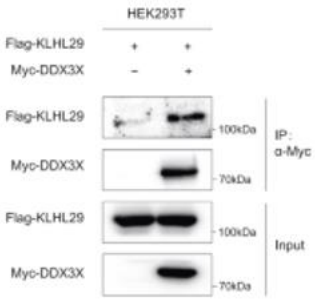

e)

g)

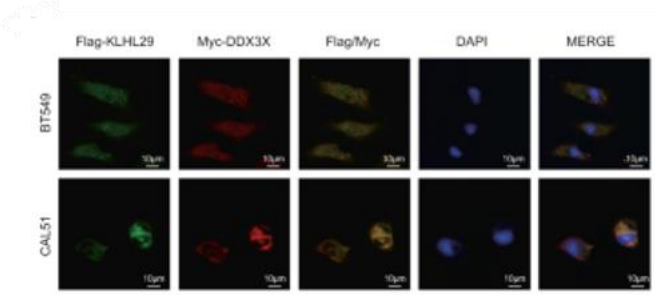

h)

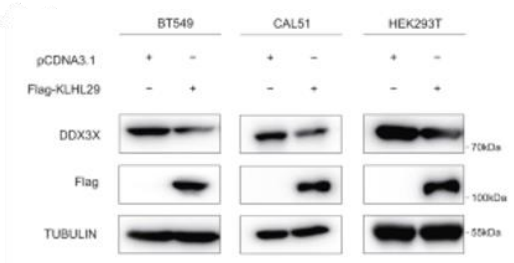

i)

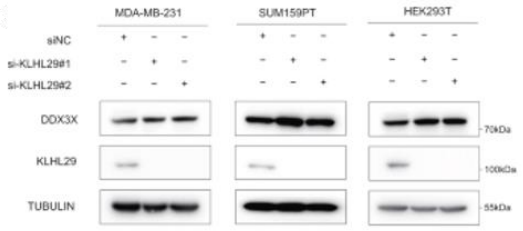

j)

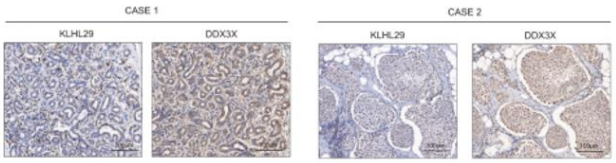

k)

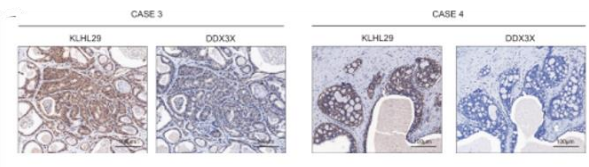

l)

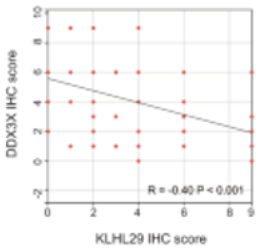

m)

Figure 4. KLHL29 associates with DDX3X and reduces DDX3X protein abundance in TNBC cells.
(a) Schematic overview of the experimental pipeline used to identify KLHL29-binding partners. BT549 and CAL51 cells stably expressing pCDH-Flag or pCDH-Flag-KLHL29 were subjected to immunoprecipitation, followed by mass spectrometry analysis.
(b) Venn diagram illustrating the overlap of proteins interacting with KLHL29. A total of 46 interacting candidates were detected in BT549 cells, whereas 69 were identified in CAL51 cells.
(c) Eight shared proteins were identified as common KLHL29 interactors in both BT549 and CAL51 cell lines.
(d, e) Reciprocal co-immunoprecipitation assays demonstrate interaction between ectopically expressed KLHL29 and DDX3X. HEK293T cells were co-transfected with Flag-KLHL29 and Myc-DDX3X constructs, followed by immunoprecipitation with anti-Flag or anti-Myc antibodies and subsequent immunoblot detection.
(f) Diagram depicting the series of KLHL29 truncation mutants generated for interaction domain analysis.
(g) Domain-mapping experiments revealed that DDX3X binds specifically to the Kelch-repeat region of KLHL29. HEK293T cells were co-transfected with Myc-DDX3X and individual Flag-tagged KLHL29 fragments prior to co-IP and western blot analyses.
(h) Confocal immunofluorescence images showing partial cytoplasmic co-distribution of Flag-KLHL29 (green) and Myc-DDX3X (red) in BT549 and CAL51 cells. Nuclei were visualized by DAPI staining (blue).
(i) Enforced KLHL29 expression resulted in decreased DDX3X protein levels in BT549 (left), CAL51 (middle), and HEK293T (right) cells.
(j) Suppression of KLHL29 expression caused accumulation of DDX3X protein in MDA-MB-231 (left), SUM159PT (middle), and HEK293T (right) cells.
(k, l) Immunohistochemical staining of KLHL29 and DDX3X in TNBC tissue sections, with representative images shown.
(m) Inverse association between KLHL29 and DDX3X expression in TNBC samples, determined using Spearman correlation analysis with two-tailed P values.

To verify the physical association between KLHL29 and DDX3X, reciprocal co-immunoprecipitation experiments were performed, confirming that exogenously expressed KLHL29 forms a complex with exogenous DDX3X in HEK293T cells **(Figures 4d and 4e).** Interaction between the endogenous proteins was additionally observed in MDA-MB-231 cells. Because KLHL29 contains a BTB/POZ domain, a BACK domain, and six Kelch-repeat motifs, a panel of deletion mutants was generated to identify the region responsible for DDX3X binding **(Figure 4f).** These analyses demonstrated that the Kelch-repeat region of KLHL29 (M4, amino acids 585–875) mediates the interaction with DDX3X **(Figure 4g).** Consistent with this finding, confocal microscopy confirmed partial cytoplasmic overlap of KLHL29 and DDX3X signals in BT549 and CAL51 cells **(Figure 4h)**, supporting a direct protein–protein interaction.

Given that many KLHL family members function as substrate adaptors within CUL3-based E3 ubiquitin ligase complexes [24, 25], we next examined whether KLHL29 modulates DDX3X protein stability. Immunoblot analysis revealed that increasing KLHL29 expression led to a marked reduction in DDX3X protein abundance **(Figure 4i),** whereas KLHL29 depletion produced the opposite effect **(Figures 4j)**. In contrast, manipulation of KLHL29 levels did not alter DDX3X transcript abundance indicating regulation occurs post-transcriptionally. Examination of TNBC clinical samples further demonstrated a negative relationship between KLHL29 and DDX3X protein expression by IHC analysis **(Figures 4k–4m).** Functional rescue assays showed that overexpression of DDX3X significantly counteracted the suppressive effects of KLHL29 on TNBC cell proliferation, migration, and invasion, indicating that KLHL29 restrains TNBC progression through inhibition of DDX3X.

KLHL29 drives ubiquitin-mediated proteasomal degradation of DDX3X

Intracellular protein turnover is primarily governed by the ubiquitin–proteasome pathway and the autophagy–lysosome system [26]. To identify the degradation route of DDX3X, TNBC cells were treated with the proteasome inhibitor MG132 or the autophagy inhibitor bafilomycin A1 (Baf-A1). DDX3X protein accumulated progressively following MG132 exposure but showed no

appreciable change after Baf-A1 treatment (**Figures 5a–5d)**, indicating dependence on the proteasome. Moreover, MG132 fully abolished the KLHL29-induced reduction of DDX3X protein levels **(Figure 5e–5g),** whereas Baf-A1 failed to restore DDX3X expression under KLHL29-overexpressing conditions. These observations demonstrate that KLHL29-mediated DDX3X degradation occurs via the ubiquitin–proteasome system rather than autophagy.

Consistently, ectopic KLHL29 expression markedly increased ubiquitination of DDX3X **(Figure 5h)**. Cycloheximide chase experiments further revealed that KLHL29 significantly shortened the half-life of DDX3X protein in BT549 **(Figure 5i and 5j),** CAL51 **(Figures 5k and 5l),** and HEK293T **(Figures 5m and 5n)** cells. Together, these findings establish that KLHL29 promotes proteasome-dependent degradation of DDX3X through ubiquitin-mediated mechanisms.

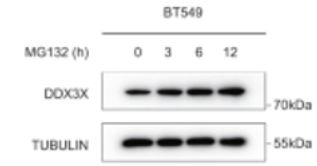

a)

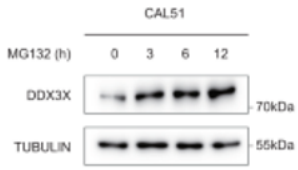

b)

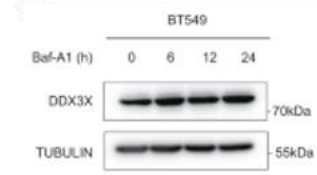

c)

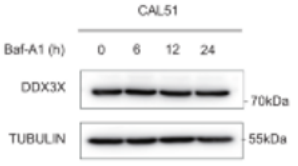

d)

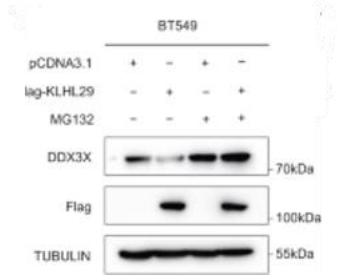

e)

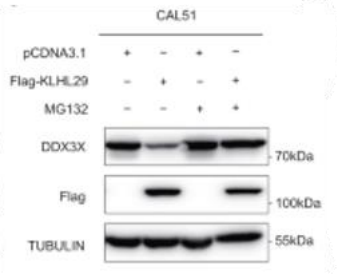

f)

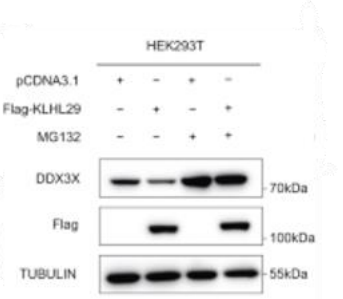

g)

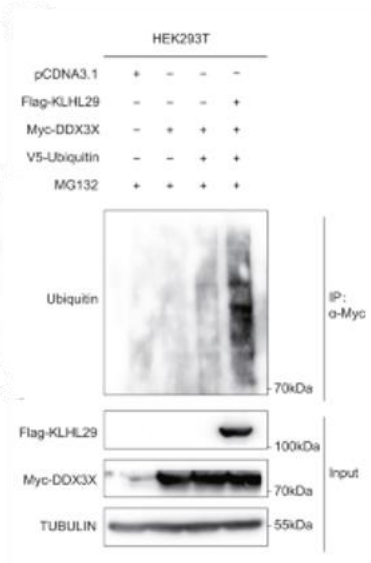

h)

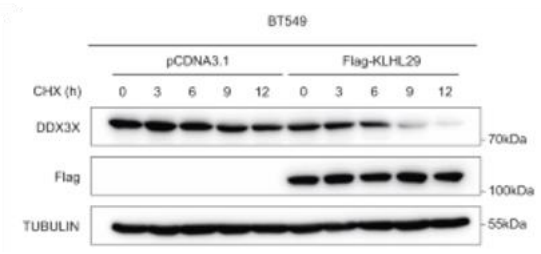

i)

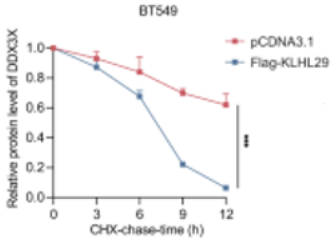

j)

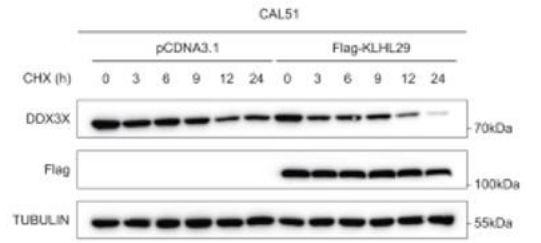

k)

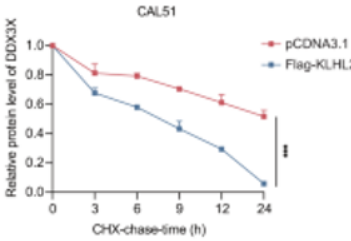

l)

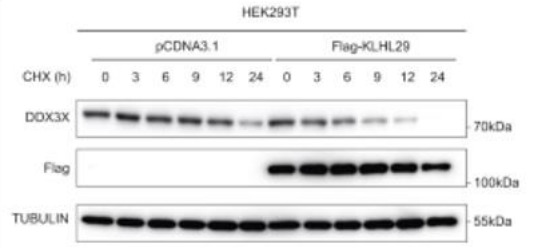

m)

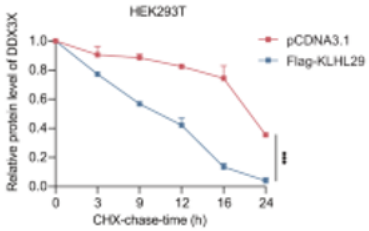

n)

Figure 5. KLHL29 facilitates the proteasomal degradation of DDX3X via ubiquitination. (a, b) In BT549 (a) and CAL51 (b) cells, treatment with 20 μM MG132 at the indicated time points caused a progressive increase in DDX3X protein. (c, d) Exposure to 200 nM Bafilomycin A1 (Baf-A1) over the same time points did not affect DDX3X levels in BT549 (c) or CAL51 (d) cells. (e–g) The presence of MG132 blocked the decrease of DDX3X mediated by KLHL29 in BT549 (e), CAL51 (F), and HEK293T (g) cells. Cells transfected with either empty vector or Flag-KLHL29 plasmid were incubated with DMSO or 20 μM MG132 for 6 hours prior to protein extraction and western blotting. (h) KLHL29 overexpression increased the ubiquitination of DDX3X. HEK293T cells were transfected with the indicated plasmids and treated with 20 μM MG132 for 6 hours before analysis. (i–n) Cycloheximide (CHX) chase assays showed that DDX3X protein half-life was significantly reduced when KLHL29 was overexpressed in BT549 (I), CAL51 (K), and HEK293T (m) cells. Cells were treated with 100 μg/mL CHX and collected at the indicated intervals. Relative quantifications (DDX3X/TUBULIN) are presented in panels J, L, and N. Statistical significance: ***$p < 0.001$ by two-tailed Student's t test.

CUL3 E3 ligase is essential for KLHL29-mediated DDX3X turnover

Kelch-like proteins frequently act as adaptors for the CUL3 E3 ubiquitin ligase through their BTB domain, targeting substrates for proteasomal degradation [24]. To determine whether CUL3 participates in KLHL29-dependent DDX3X degradation, reciprocal co-immunoprecipitation experiments were performed. KLHL29 was found to associate with CUL3 **(Figures 6a and 6b)**, with th0e interaction localized to the BTB domain **(Figure 6c)**. Endogenous KLHL29–CUL3 interaction was also confirmed in MDA-MB-231 cells.

RNA-seq analyses from FUSCC-TNBC and TCGA datasets revealed that CUL3 expression was significantly lower in TNBC tumors relative to adjacent normal tissue. Overexpressing CUL3 enhanced DDX3X proteasomal degradation, which could be blocked by MG132 treatment **(Figures 6d–6f).** Conversely, knocking down CUL3 prevented KLHL29 from reducing DDX3X protein levels. Furthermore, ectopic CUL3 increased DDX3X ubiquitination, an effect that was potentiated by simultaneous KLHL29 overexpression **(Figure 6g).**

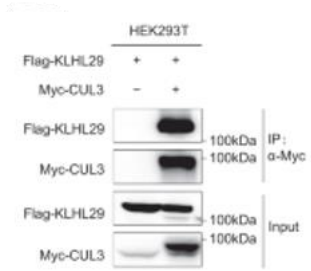

a)

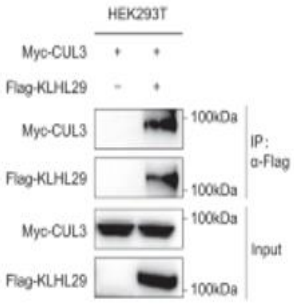

b)

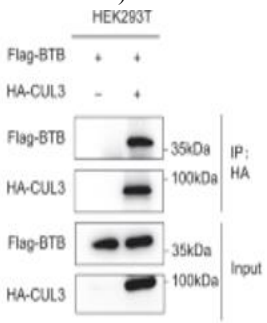

c)

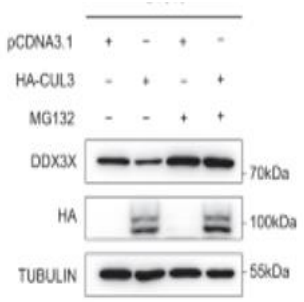

d)

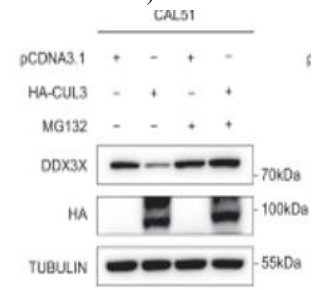

e)

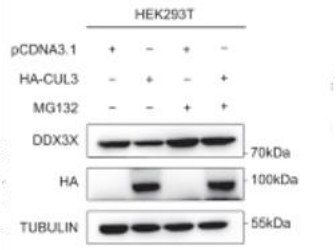

f)

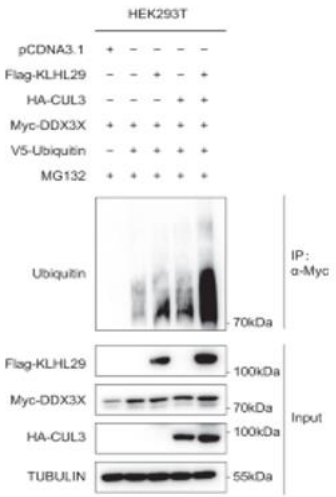

g)

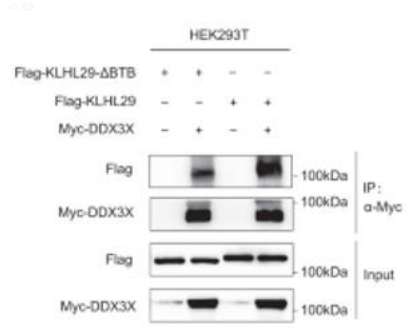
HEK293T
Flag-KLHL29-ΔBTB + + − −
Flag-KLHL29 − − + +
Myc-DDX3X − + − +
Flag
Myc-DDX3X
Flag
Myc-DDX3X
100kDa
100kDa
100kDa
100kDa
IP: α-Myc
Input

h)

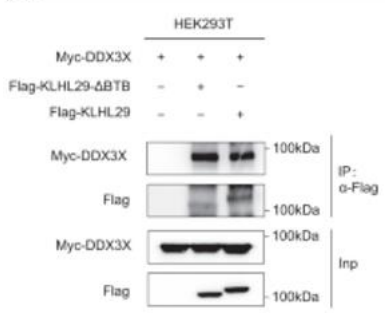
HEK293T
Myc-DDX3X + + +
Flag-KLHL29-ΔBTB − + −
Flag-KLHL29 − − +
Myc-DDX3X
Flag
Myc-DDX3X
Flag
100kDa
100kDa
100kDa
100kDa
IP: α-Flag
Inp

i)

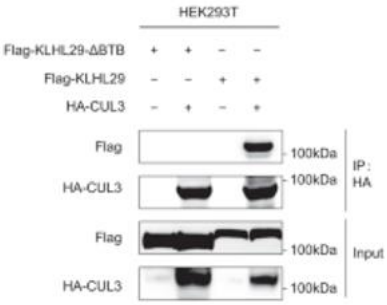
HEK293T
Flag-KLHL29-ΔBTB + + − −
Flag-KLHL29 − − + +
HA-CUL3 − + − +
Flag
HA-CUL3
Flag
HA-CUL3
100kDa
100kDa
100kDa
100kDa
IP: HA
Input

j)

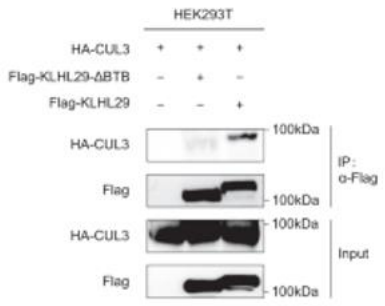
HEK293T
HA-CUL3 + + +
Flag-KLHL29-ΔBTB − + −
Flag-KLHL29 − − +
HA-CUL3
Flag
HA-CUL3
Flag
100kDa
100kDa
100kDa
100kDa
IP: α-Flag
Input

k)

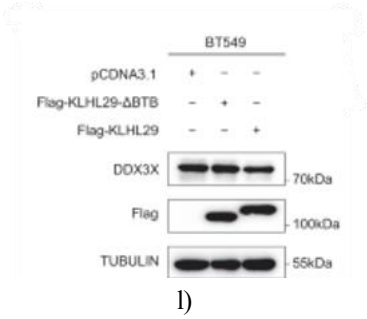
BT549
pCDNA3.1 + − −
Flag-KLHL29-ΔBTB − + −
Flag-KLHL29 − − +
DDX3X
Flag
TUBULIN
70kDa
100kDa
55kDa

l)

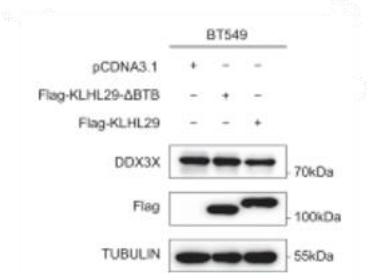
BT549
pCDNA3.1 + − −
Flag-KLHL29-ΔBTB − + −
Flag-KLHL29 − − +
DDX3X
Flag
TUBULIN
70kDa
100kDa
55kDa

m)

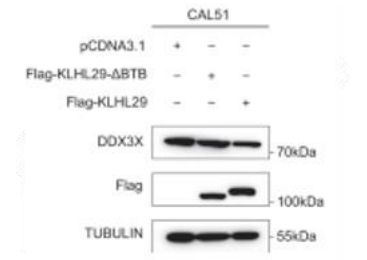
CAL51
pCDNA3.1 + − −
Flag-KLHL29-ΔBTB − + −
Flag-KLHL29 − − +
DDX3X
Flag
TUBULIN
70kDa
100kDa
55kDa

n)

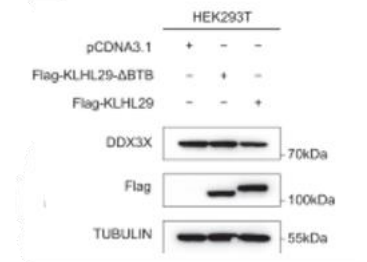
HEK293T
pCDNA3.1 + − −
Flag-KLHL29-ΔBTB − + −
Flag-KLHL29 − − +
DDX3X
Flag
TUBULIN
70kDa
100kDa
55kDa

o)

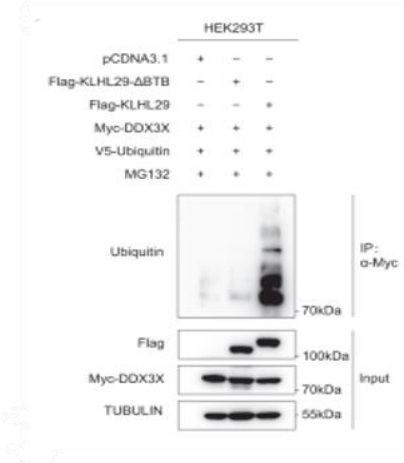

p)

Figure 6. The BTB motif of KLHL29 mediates CUL3-dependent DDX3X degradation.

(a, b) In HEK293T cells, co-immunoprecipitation assays demonstrate that exogenous KLHL29 forms a complex with Myc-CUL3 after transfection with Flag-KLHL29 and Myc-CUL3 plasmids.

(c) Mapping experiments reveal that the BTB domain is essential for KLHL29 to engage with CUL3.

(d–f) Overexpression of CUL3 reduces DDX3X protein in BT549 (D), CAL51 (e), and HEK293T (f) cells, and this effect is reversed by 20 μM MG132 applied for 6 hours. Cells transfected with empty vector or HA-CUL3 were analyzed by western blotting.

(g) KLHL29 amplifies CUL3-mediated ubiquitination of DDX3X.

(h, i) The KLHL29 variant lacking the BTB domain (KLHL29-ΔBTB) retains binding to DDX3X in HEK293T cells transfected with Myc-DDX3X and Flag-KLHL29-ΔBTB or Flag-KLHL29.

(j, k) KLHL29-ΔBTB is unable to interact with CUL3 in HEK293T cells co-transfected with HA-CUL3 and Flag-KLHL29-ΔBTB or Flag-KLHL29.

(l) Only intact KLHL29 promotes CUL3-DDX3X association when co-expressed with Myc-DDX3X and HA-CUL3; KLHL29-ΔBTB cannot.

(m–o) KLHL29-ΔBTB fails to decrease DDX3X protein in BT549 (M), CAL51 (N), and HEK293T (O) cells.

(p) KLHL29-ΔBTB does not enhance DDX3X ubiquitination.

To determine the functional contribution of the BTB motif, a deletion mutant (KLHL29-ΔBTB) was generated. Despite retaining DDX3X binding (**Figures 6 and 6i)**, KLHL29-ΔBTB cannot recruit CUL3 **(Figures 6j and 6k)**, indicating that the BTB motif is critical for connecting DDX3X to the ubiquitin ligase. In contrast, full-length KLHL29 robustly increases CUL3-DDX3X interaction **(Figure 6l),** lowers DDX3X levels **(Figures 6m–6o),** and promotes ubiquitination **(Figure 6p).** Only full-length KLHL29 effectively inhibits TNBC cell proliferation, migration, and invasion. These results show that the BTB domain enables KLHL29 to target DDX3X for degradation through CUL3, suppressing TNBC progression.

KLHL29–DDX3X axis regulates TNBC cell cycle progression

DDX3X, an RNA-binding protein, regulates transcription, pre-mRNA splicing, and mRNP assembly [27, 28]. To explore its molecular role in TNBC, transcriptomic profiling was performed. Gene set enrichment analysis (GSEA) linked DDX3X to cell cycle-related pathways in MDA-MB-231 and SUM159PT cells **(Figure 7a).** KEGG and GO analyses showed enrichment of cell cycle genes upon DDX3X depletion. Using ssGSEA on the FUSCC-TNBC dataset, KLHL29 expression correlated with dysregulation of cell cycle genes **(Figure 7b),** suggesting a KLHL29–DDX3X regulatory axis.

Flow cytometry confirmed these predictions. Silencing DDX3X caused G0/G1 accumulation in MDA-MB-231 and SUM159PT cells **(Figures 7c and 7d).** Likewise, KLHL29 overexpression led to G0/G1 arrest **(Figures 7e, and 7e)**, whereas KLHL29 knockdown accelerated G1/S transition **(Figures 7g and 6h).** Re-introducing DDX3X reversed the G0/G1 arrest induced by KLHL29 **(Figures 7i and 7j),** demonstrating that KLHL29 controls TNBC cell cycle progression through DDX3X.

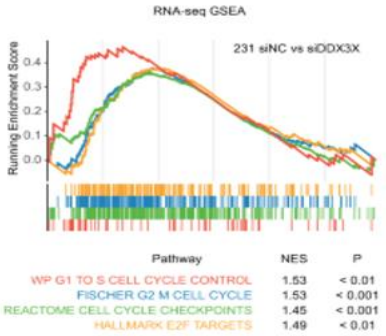

a)

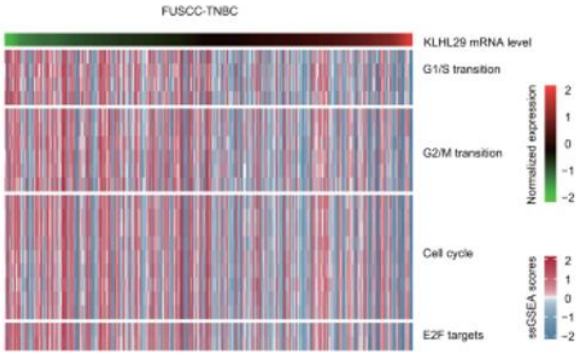
FUSCC-TNBC
KLHL29 mRNA level
G1/S transition
G2/M transition
Cell cycle
E2F targets
Normalized expression
ssGSEA scores

b)

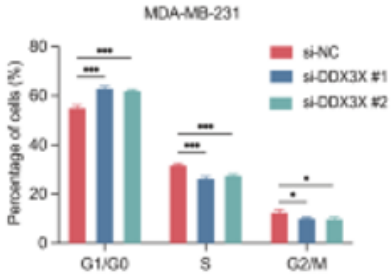
MDA-MB-231
si-NC
si-DDX3X #1
si-DDX3X #2
Percentage of cells (%)
G1/G0
S
G2/M

c)

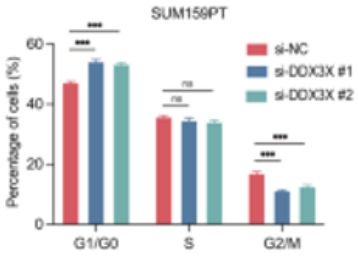
SUM159PT
si-NC
si-DDX3X #1
si-DDX3X #2
Percentage of cells (%)
G1/G0
S
G2/M

d)

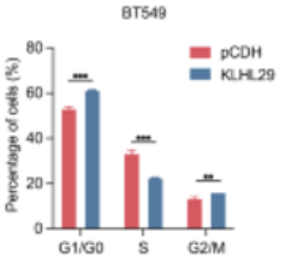
BT549
pCDH
KLHL29
Percentage of cells (%)
G1/G0
S
G2/M

e)

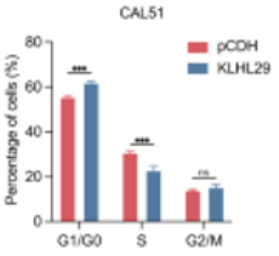
CAL51
pCDH
KLHL29
Percentage of cells (%)
G1/G0
S
G2/M

f)

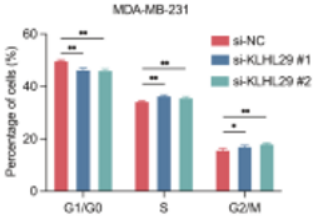
MDA-MB-231
si-NC
si-KLHL29 #1
si-KLHL29 #2
Percentage of cells (%)
G1/G0
S
G2/M

g)

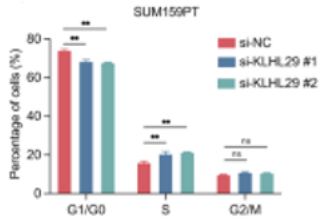
SUM159PT
si-NC
si-KLHL29 #1
si-KLHL29 #2
Percentage of cells (%)
G1/G0
S
G2/M

h)

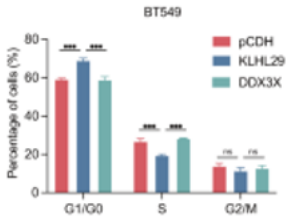
BT549
pCDH
KLHL29
DDX3X
Percentage of cells (%)
G1/G0
S
G2/M

i)

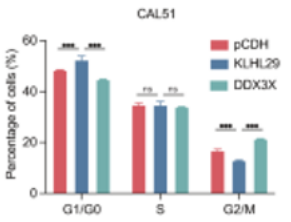
CAL51
pCDH
KLHL29
DDX3X
Percentage of cells (%)
G1/G0
S
G2/M

j)

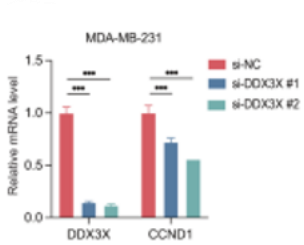

k)

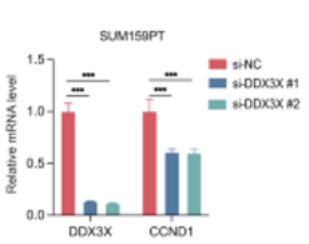

l)

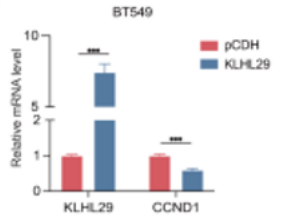

m)

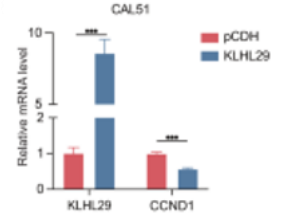

n)

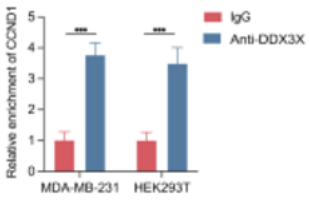

o)

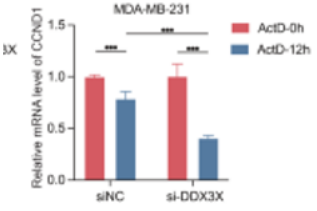

p)

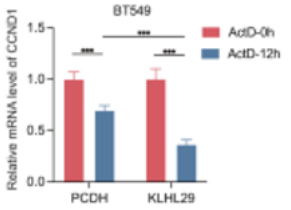

q)

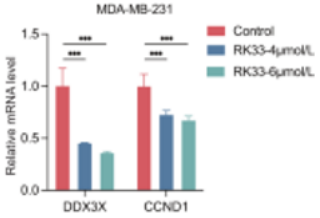

r)

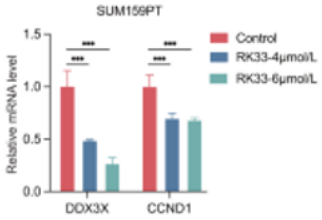

s)

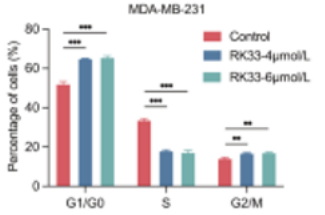

t)

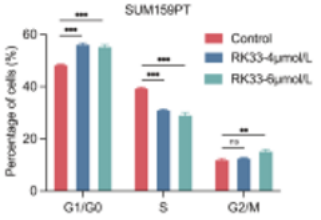

u)

Figure 7. Regulation of TNBC cell cycle by the KLHL29–DDX3X pathway

(a) GSEA shows that knockdown of DDX3X in MDA-MB-231 cells leads to enrichment in pathways related to cell cycle control.

(b) ssGSEA analysis indicates a correlation between KLHL29 transcript levels and cell cycle gene expression in the FUSCC-TNBC dataset.
(c, d) Flow cytometric quantification using PI staining demonstrates that silencing DDX3X causes accumulation of cells in G0/G1 phase in MDA-MB-231 (c) and SUM159PT (d) lines. Percentages in G1, S, and G2/M phases are reported.
(e, f) Forced KLHL29 expression in BT549 (e) and CAL51 (f) cells similarly triggers G0/G1 phase accumulation.
(g, h) Conversely, KLHL29 knockdown reduces the G0/G1 population in MDA-MB-231 (g) and SUM159PT (H) cells.
(i, j) Restoration of DDX3X rescues the G0/G1 arrest induced by KLHL29 overexpression in BT549 (i) and CAL51 (j) cells.
(k, l) RT-qPCR confirms that CCND1 mRNA is decreased following DDX3X depletion in MDA-MB-231 (k) and SUM159PT (l).
(m, n) KLHL29 overexpression also downregulates CCND1 transcripts in BT549 (m) and CAL51 (n) cells.
(o) RIP assays verify direct binding of DDX3X to CCND1 mRNA in MDA-MB-231 and HEK293T cells transfected with Myc-DDX3X.
(p, q) Treatment with Actinomycin D (5 μg/ml) demonstrates that either DDX3X depletion (p) or KLHL29 overexpression (Q) destabilizes CCND1 mRNA.
(r, s) RK33 treatment lowers DDX3X and CCND1 transcript levels in MDA-MB-231 (R) and SUM159PT (s) cells.
(t, u) Flow cytometry indicates that RK33 triggers G0/G1 arrest in both MDA-MB-231 (t) and SUM159PT (u).
*p < 0.05, **p < 0.01, ***p < 0.001, ns = not significant (two-tailed Student's t test).

Mechanistically, transcriptomic data and RT-qPCR validation reveal that DDX3X knockdown suppresses CCND1, CCNE1, and CCNA2, key cyclins promoting G1/S transition [29] **(Figure 7k and 7l)**. KLHL29 overexpression similarly reduces expression of these cyclins **(Figures 7m and 7n)**. RIP experiments show DDX3X binds directly to CCND1 mRNA **(Figure 7o),** stabilizing it. Both DDX3X knockdown and KLHL29 overexpression accelerate CCND1 mRNA decay in the presence of Actinomycin D (5 μg/ml); (**Figures. 7p and 7q).** RK33, a DDX3X-targeting inhibitor with activity in breast, lung, and sarcoma models [30–32], significantly diminishes DDX3X and CCND1 expression **(Figure 7r and 7s)** and induces G0/G1 arrest **(Figures 7t and 7u)**, highlighting the KLHL29–DDX3X axis as a critical regulator of cell cycle genes in TNBC.

Combination therapy: RK33 plus platinum agents suppresses TNBC growth

Platinum chemotherapy remains standard for TNBC, with the G1/S checkpoint critical for DNA damage response and drug sensitivity [33, 34]. We tested whether inhibiting DDX3X enhances platinum sensitivity via cell cycle modulation. RK33 treatment significantly reduced TNBC cell viability, with DDX3X depletion or KLHL29 overexpression increasing IC50. Organoids derived from TNBC patients with high DDX3X or low KLHL29 showed heightened RK33 sensitivity.

Combination treatments with RK33 plus cisplatin or carboplatin inhibited TNBC proliferation more than single agents **(Figures 8a–8D).** CI analysis confirmed synergistic interactions (CI < 1) across multiple cell lines for RK33 plus cisplatin **(Figures 8e–8l),** and similar synergy was observed for carboplatin.

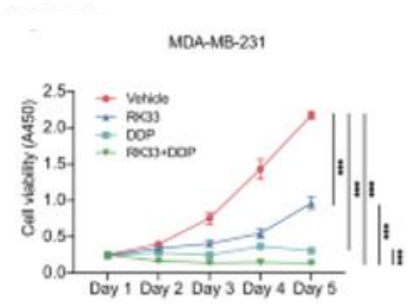

a)

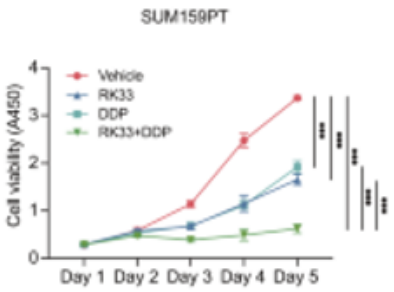

b)

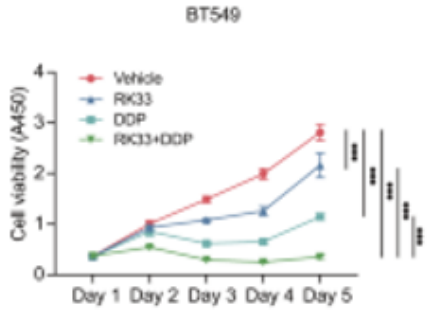
BT549
Vehicle
RK33
DDP
RK33+DDP
Cell viability (A450)
Day 1 Day 2 Day 3 Day 4 Day 5

c)

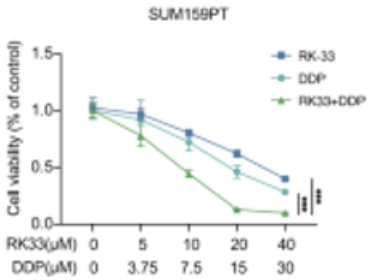
SUM159PT
RK-33
DDP
RK33+DDP
Cell viability (% of control)
RK33(μM) 0 5 10 20 40
DDP(μM) 0 3.75 7.5 15 30

g)

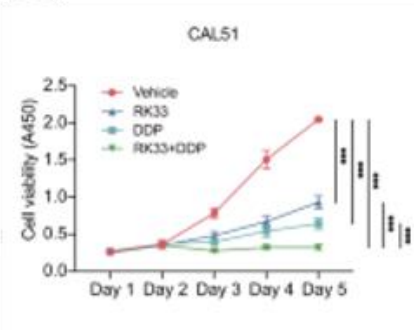
CAL51
Vehicle
RK33
DDP
RK33+DDP
Cell viability (A450)
Day 1 Day 2 Day 3 Day 4 Day 5

d)

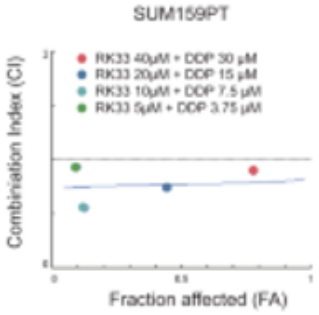
SUM159PT
RK33 40μM + DDP 30 μM
RK33 20μM + DDP 15 μM
RK33 10μM + DDP 7.5 μM
RK33 5μM + DDP 3.75 μM
Combination Index (CI)
Fraction affected (FA)

h)

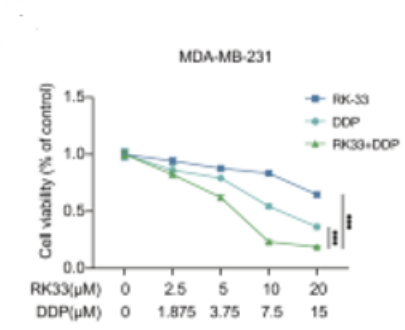
MDA-MB-231
RK-33
DDP
RK33+DDP
Cell viability (% of control)
RK33(μM) 0 2.5 5 10 20
DDP(μM) 0 1.875 3.75 7.5 15

e)

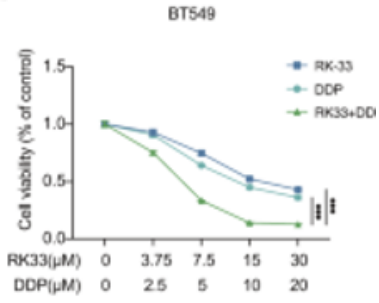
BT549
RK-33
DDP
RK33+DDP
Cell viability (% of control)
RK33(μM) 0 3.75 7.5 15 30
DDP(μM) 0 2.5 5 10 20

i)

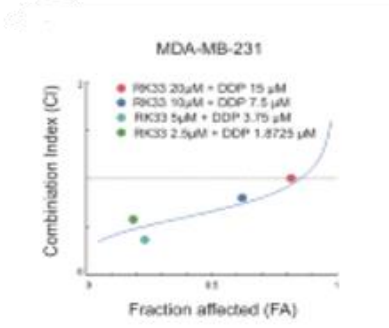
MDA-MB-231
RK33 20μM + DDP 15 μM
RK33 10μM + DDP 7.5 μM
RK33 5μM + DDP 3.75 μM
RK33 2.5μM + DDP 1.8725 μM
Combination Index (CI)
Fraction affected (FA)

f)

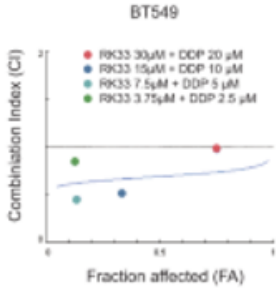
BT549
RK33 30μM + DDP 20 μM
RK33 15μM + DDP 10 μM
RK33 7.5μM + DDP 5 μM
RK33 3.75μM + DDP 2.5 μM
Combination Index (CI)
Fraction affected (FA)

j)

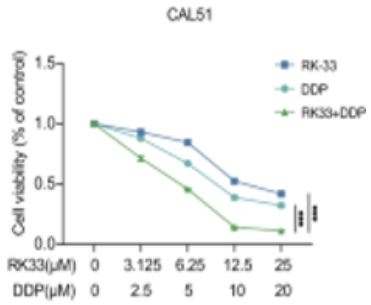
CAL51
Cell viability (% of control)
RK-33
DDP
RK33+DDP
RK33(μM) 0 3.125 6.25 12.5 25
DDP(μM) 0 2.5 5 10 20

k)

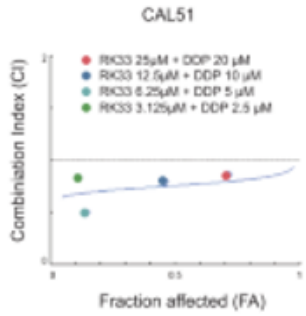
CAL51
RK33 25μM + DDP 20 μM
RK33 12.5μM + DDP 10 μM
RK33 6.25μM + DDP 5 μM
RK33 3.125μM + DDP 2.5 μM
Combination Index (CI)
Fraction affected (FA)

l)

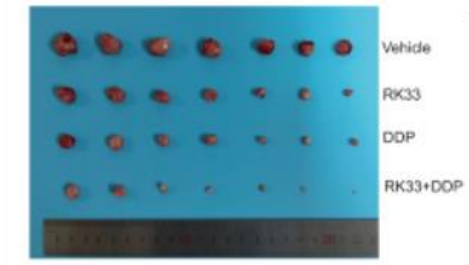
Vehicle
RK33
DDP
RK33+DDP

m)

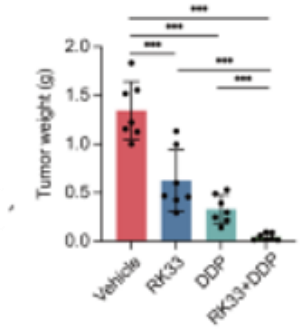
Tumor weight (g)
Vehicle
RK33
DDP
RK33+DDP

n)

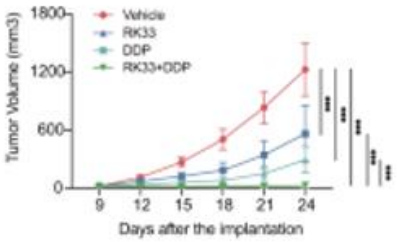
Vehicle
RK33
DDP
RK33+DDP
Tumor Volume (mm3)
Days after the implantation

o)

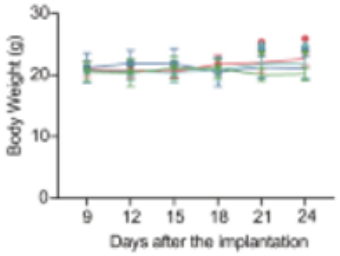
Body Weight (g)
Days after the implantation

p)

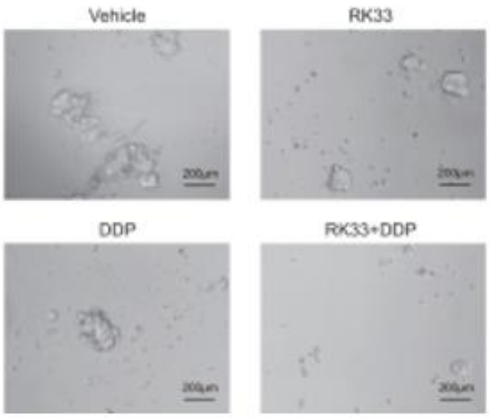
Vehicle
RK33
DDP
RK33+DDP

q)

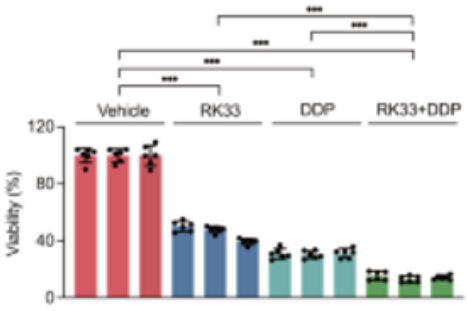
Vehicle
RK33
DDP
RK33+DDP
Viability (%)

r)

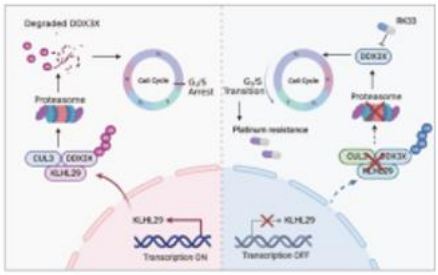

s)

Figure 8. RK33 combined with cisplatin suppresses TNBC progression both in vitro and in vivo
(a–d) Single-agent treatment with either RK33 or cisplatin reduces proliferation of MDA-MB-231 (a), SUM159PT (b), BT549 (c), and CAL51 (d) cells relative to vehicle control, as measured by Cell Counting Kit-8 assays. Notably, simultaneous exposure to RK33 and cisplatin more strongly inhibits TNBC cell growth compared with either drug alone.
(e, f) Synergistic suppression of MDA-MB-231 cell proliferation is observed when RK33 is combined with cisplatin, as confirmed by cell viability assays (e) and Chou-Talalay CI analysis (f).
(g, h) SUM159PT cells exhibit similar synergistic growth inhibition with the RK33/cisplatin combination.
(i, j) BT549 cells are also more effectively suppressed by the combination treatment.
(k, l) CAL51 cells show synergistic growth inhibition under RK33 plus cisplatin treatment.
(m–p) In vivo, the co-administration of RK33 and cisplatin strongly reduces the growth of orthotopically implanted MDA-MB-231 xenografts in BALB/c female nude mice (n = 7 per group). Representative tumor images (m), tumor growth curves (n), tumor weights (o), and mouse body weights (p) are presented.
(q, r) TNBC patient-derived organoids (PDOs) treated with the RK33/cisplatin combination show pronounced growth suppression. Representative organoid images post-treatment (q) and quantification of viability via CellTiter-Glo 3D assays (r) are displayed.
(s) Schematic model: KLHL29 recruits the CUL3 E3-ligase, promoting ubiquitination and proteasomal degradation of DDX3X, resulting in G0/G1 cell cycle arrest. Pharmacological inhibition of DDX3X with RK33 sensitizes TNBC to platinum chemotherapy.

To validate the translational relevance, MDA-MB-231 xenografts in BALB/c-nude mice were treated with vehicle, RK33, platinum agents (cisplatin or carboplatin), or the combination. While single-agent treatments partially inhibited tumor growth, the RK33/platinum combination led to more pronounced tumor suppression, as indicated by tumor volume, growth rate, and weight **(Figures 8m–8o).** Treatment was well tolerated, as body weights remained similar to controls **(Figure 8p).** PDO assays further corroborated the enhanced anti-TNBC efficacy of the combination therapy **(Figure 8q and 8r)**. These findings demonstrate that RK33 plus platinum chemotherapy efficiently suppresses TNBC in both cell lines and preclinical models.

To assess whether RK33-mediated sensitization depends on G1/S cell cycle control, RK33 was combined with paclitaxel. Cell viability assays showed that RK33 plus paclitaxel inhibited TNBC proliferation more than RK33 alone. However, CI analysis revealed no synergistic effect (CI > 1) across multiple TNBC cell lines, indicating that G1/S checkpoint modulation is critical for RK33 combination efficacy.

Triple-negative breast cancer (TNBC) progression and resistance to chemotherapy are driven by complex gene regulatory networks. In this study, we identify the KLHL29-DDX3X signaling pathway as a critical regulator of TNBC growth and treatment response. KLHL29 is expressed at significantly lower levels in TNBC tissues compared with matched normal tissues, and reduced KLHL29 correlates with poor clinical outcomes **(Figure 1)**. Functional assays reveal that KLHL29 overexpression suppresses, whereas its depletion accelerates, TNBC proliferation and metastatic behaviors **(Figures. 2 and 3).** Mechanistically, KLHL29 serves as an adaptor connecting the CUL3 E3-ligase to DDX3X, enhancing DDX3X degradation via the proteasome, which subsequently decreases cyclin expression and triggers G0/G1 cell cycle arrest **(Figures. 4–7)**. Because TNBC typically features low KLHL29 and high DDX3X, pharmacological inhibition of DDX3X with RK33 in combination with platinum agents results in synergistic anti-tumor activity in vitro and in vivo **(Figure 8).**

KLHL29 is part of the KLHL protein family, which generally contains a BTB/POZ domain, a BACK domain, and six Kelch repeats. These proteins regulate diverse cellular processes by interacting with specific substrates. In the CUL3-KLHL ubiquitin ligase complex, the BTB domain engages CUL3, while the Kelch repeats recruit target proteins [24]. Using mass spectrometry and co-immunoprecipitation assays, we identified the RNA helicase DDX3X as a previously unrecognized KLHL29

partner **(Figures 4a–4h).** KLHL29 recruits CUL3 to trigger DDX3X ubiquitination and proteasomal degradation, as evidenced by multiple lines of support **(Figures 4–6)**. First, KLHL29 interacts with CUL3 in TNBC and HEK293T cells **(Figures 6a–6c).** Second, KLHL29 increases the CUL3-DDX3X interaction **(Figure 6l).** Third, CUL3 promotes DDX3X ubiquitination and proteasomal breakdown, further augmented by KLHL29 overexpression **(Figures 6d–6g)**. Fourth, the BTB domain is essential for CUL3 recruitment, as KLHL29 lacking this domain (KLHL29-ΔBTB) cannot bind CUL3, enhance CUL3-DDX3X interaction, or drive DDX3X degradation **(Figures 6h–6p)**. Finally, KLHL29 levels inversely correlate with DDX3X expression in patient samples **(Figures 4k–4m).** Collectively, these findings highlight KLHL29 as a previously unrecognized tumor suppressor in TNBC.

DDX3X, a member of the DEAD-box helicase family [35], participates broadly in RNA metabolism, including transcription, splicing, and mRNP assembly [36–40]. Its function in cancer is context-dependent, with oncogenic or tumor-suppressive roles depending on tumor type [28, 41–43]. In TNBC, DDX3X is overexpressed relative to adjacent normal tissue, and high expression correlates with poor prognosis. Functional experiments show that DDX3X acts as an oncogene: overexpression reverses the inhibitory effects of KLHL29 on TNBC proliferation and migration**.** The oncogenic activity of DDX3X is partly mediated by its ability to upregulate cyclin genes and promote G1/S cell cycle progression **(Figure 7c–7n).** In particular, DDX3X binds CCND1 mRNA, stabilizing the transcript **(Figures 7o–7q).** Knockdown of DDX3X or inhibition with RK33 leads to G0/G1 arrest **(Figures 7c–7j, 7t and 7u),** suggesting that DDX3X is a viable therapeutic target in TNBC.

Platinum-based chemotherapy is a key treatment for TNBC in neoadjuvant and metastatic settings [44–46]. Cell cycle control strongly influences platinum sensitivity [33, 34, 47], and cyclin overexpression, such as CCND1 or CCNE1 amplification, can mediate resistance [48–50]. Prior studies indicated that ~50% of TNBC cases exhibit CCND1 and CCNE1 amplification or overexpression [28], supporting the rationale for targeting DDX3X to reduce cyclin expression and enhance chemosensitivity. Indeed, combination therapy with RK33 and cisplatin or carboplatin synergistically inhibits TNBC growth in vitro, xenografts, and PDO models **(Figure 8)**. Highlighting a promising combinatorial strategy for tumors with low KLHL29 and high DDX3X/cyclins.

Conclusion

In conclusion, KLHL29 functions as a tumor suppressor in TNBC by recruiting CUL3 to promote DDX3X ubiquitination and proteasomal degradation, repressing cyclin gene expression and inducing G0/G1 arrest. TNBC cells with low KLHL29 and high DDX3X are sensitized to platinum therapy via RK33-mediated DDX3X inhibition. These findings offer a mechanistic basis for developing novel combination therapies targeting the KLHL29-DDX3X axis.

Acknowledgments: We thank the laboratory members for active and helpful discussion. This work was supported by the National Natural Science Foundation of China (82373231 to YX, 82273098 and 82072879 to XZ, 82173022 to QH, and 82203786 to MW), and the Natural Science Foundation of Liaoning Province of China (2022-YGJC-68 and 2023-BS-105) and Chinese Young Breast Experts Research Project (CYBER-2021-A02 and CYBER-2022-001).

Conflict of Interest: None

Financial Support: None

Ethics Statement: None

References

1. Siegel RL, Miller KD, Fuchs HE, Jemal A. Cancer statistics, 2022. CA Cancer J Clin. 2022;72:7–33.
2. Metzger-Filho O, Tutt A, de Azambuja E, Saini KS, Viale G, Loi S, et al. Dissecting the heterogeneity of triple-negative breast cancer. J Clin Oncol. 2012;30:1879–87.
3. Cancer Genome Atlas Network. Comprehensive molecular portraits of human breast tumours. Nature. 2012;490:61–70.
4. Ge J, Zuo W, Chen Y, Shao Z, Yu K. The advance of adjuvant treatment for triple-negative breast cancer. Cancer Biol Med. 2021;19:187–201.
5. Garrido-Castro AC, Lin NU, Polyak K. Insights into molecular classifications of triple-negative breast cancer: improving patient selection for treatment. Cancer Discov. 2019;9:176–98.

6. Dent R, Trudeau M, Pritchard KI, Hanna WM, Kahn HK, Sawka CA, et al. Triple-negative breast cancer: clinical features and patterns of recurrence. Clin Cancer Res. 2007;13:4429–34.
7. Bianchini G, Balko JM, Mayer IA, Sanders ME, Gianni L. Triple-negative breast cancer: challenges and opportunities of a heterogeneous disease. Nat Rev Clin Oncol. 2016;13:674–90.
8. Leon-Ferre RA, Goetz MP. Advances in systemic therapies for triple negative breast cancer. BMJ. 2023;381:e071674.
9. Derakhshan F, Reis-Filho JS. Pathogenesis of triple-negative breast cancer. Annu Rev Pathol. 2022;17:181–204.
10. Denkert C, Liedtke C, Tutt A, von Minckwitz G. Molecular alterations in triple-negative breast cancer-the road to new treatment strategies. Lancet. 2017;389:2430–42.
11. Jiang Y-Z, Ma D, Suo C, Shi J, Xue M, Hu X, et al. Genomic and transcriptomic landscape of triple-negative breast cancers: subtypes and treatment strategies. Cancer Cell. 2019;35:428–40.e5.
12. Gong T-Q, Jiang Y-Z, Shao C, Peng W-T, Liu M-W, Li D-Q, et al. Proteome-centric cross-omics characterization and integrated network analyses of triple-negative breast cancer. Cell Rep. 2022;38:110460.
13. Yu T-J, Liu Y-Y, Li X-G, Lian B, Lu X-X, Jin X, et al. PDSS1-mediated activation of CAMK2A-STAT3 signaling promotes metastasis in triple-negative breast cancer. Cancer Res. 2021;81:5491–505.
14. Chen Y-Y, Ge J-Y, Zhu S-Y, Shao Z-M, Yu K-D. Copy number amplification of ENSA promotes the progression of triple-negative breast cancer via cholesterol biosynthesis. Nat Commun. 2022;13:791.
15. Yang Y-S, Jin X, Li Q, Chen Y-Y, Chen F, Zhang H, et al. Superenhancer drives a tumor-specific splicing variant of MARCO to promote triple-negative breast cancer progression. Proc Natl Acad Sci USA. 2022;119:e2207201119.
16. Shi X, Xiang S, Cao J, Zhu H, Yang B, He Q, et al. Kelch-like proteins: physiological functions and relationships with diseases. Pharmacol Res. 2019;148:104404.
17. Adams J, Kelso R, Cooley L. The kelch repeat superfamily of proteins: propellers of cell function. Trends Cell Biol. 2000;10:17–24.
18. Dhanoa BS, Cogliati T, Satish AG, Bruford EA, Friedman JS. Update on the Kelch-like (KLHL) gene family. Hum Genomics. 2013;7:13.
19. Li X, Yang K-B, Chen W, Mai J, Wu X-Q, Sun T, et al. CUL3 (cullin 3)-mediated ubiquitination and degradation of BECN1 (beclin 1) inhibit autophagy and promote tumor progression. Autophagy. 2021;17:4323–40.
20. Yuan W-C, Lee Y-R, Huang S-F, Lin Y-M, Chen T-Y, Chung H-C, et al. A Cullin3-KLHL20 Ubiquitin ligase-dependent pathway targets PML to potentiate HIF-1 signaling and prostate cancer progression. Cancer Cell. 2011;20:214–28.
21. Fu A-B, Xiang S-F, He Q-J, Ying M-D. Kelch-like proteins in the gastrointestinal tumors. Acta Pharmacol Sin. 2023;44:931–9.
22. Chen J, Ou Y, Yang Y, Li W, Xu Y, Xie Y, et al. KLHL22 activates amino-acid-dependent mTORC1 signalling to promote tumorigenesis and ageing. Nature. 2018;557:585–9.
23. achs N, de Ligt J, Kopper O, Gogola E, Bounova G, Weeber F, et al. A living biobank of breast cancer organoids captures disease heterogeneity. Cell. 2018;172:373–86.e10.
24. Xiang S, Shi X, Chen P, Chen Y, Bing S, Jin X, et al. Targeting Cul3-scaffold E3 ligase complex via KLHL substrate adaptors for cancer therapy. Pharmacol Res. 2021;169:105616.
25. Pintard L, Willems A, Peter M. Cullin-based ubiquitin ligases: Cul3-BTB complexes join the family. EMBO J. 2004;23:1681–7.
26. Kwon YT, Ciechanover A. The ubiquitin code in the ubiquitin-proteasome system and autophagy. Trends Biochem Sci. 2017;42:873–86.
27. Shen H, Yanas A, Owens MC, Zhang C, Fritsch C, Fare CM, et al. Sexually dimorphic RNA helicases DDX3X and DDX3Y differentially regulate RNA metabolism through phase separation. Mol Cell. 2022;82:2588–603.e9.
28. Mo J, Liang H, Su C, Li P, Chen J, Zhang B. DDX3X: structure, physiologic functions and cancer. Mol Cancer. 2021;20:38.
29. Bertoli C, Skotheim JM, de Bruin RAM. Control of cell cycle transcription during G1 and S phases. Nat Rev Mol Cell Biol. 2013;14:518–28.
30. Kondaskar A, Kondaskar S, Kumar R, Fishbein JC, Muvarak N, Lapidus RG, et al. Novel, broad spectrum anti-cancer agents containing the Tricyclic

5:7:5-Fused Diimidazodiazepine ring system. ACS Med Chem Lett. 2010;2:252–6.
31. Bol GM, Vesuna F, Xie M, Zeng J, Aziz K, Gandhi N, et al. Targeting DDX3 with a small molecule inhibitor for lung cancer therapy. EMBO Mol Med. 2015;7:648–69.
32. Xie M, Vesuna F, Tantravedi S, Bol GM, Heerma van Voss MR, Nugent K, et al. RK-33 radiosensitizes prostate cancer cells by blocking the RNA Helicase DDX3. Cancer Res. 2016;76:6340–50.
33. Huang C-S, Zhu Y-Q, Xu Q-C, Chen S, Huang Y, Zhao G, et al. YTHDF2 promotes intrahepatic cholangiocarcinoma progression and desensitises cisplatin treatment by increasing CDKN1B mRNA degradation. Clin Transl Med. 2022;12:e848.
34. Replogle JM, Zhou W, Amaro AE, McFarland JM, Villalobos-Ortiz M, Ryan J, et al. Aneuploidy increases resistance to chemotherapeutics by antagonizing cell division. Proc Natl Acad Sci USA. 2020;117:30566–76.
35. Bol GM, Xie M, Raman V. DDX3, a potential target for cancer treatment. Mol Cancer. 2015;14:188.
36. Merz C, Urlaub H, Will CL, Lührmann R. Protein composition of human mRNPs spliced in vitro and differential requirements for mRNP protein recruitment. RNA. 2007;13:116–28.
37. Yedavalli VSRK, Neuveut C, Chi Y-H, Kleiman L, Jeang K-T. Requirement of DDX3 DEAD box RNA helicase for HIV-1 Rev-RRE export function. Cell. 2004;119:381–92.
38. Askjaer P, Bachi A, Wilm M, Bischoff FR, Weeks DL, Ogniewski V, et al. RanGTP-regulated interactions of CRM1 with nucleoporins and a shuttling DEAD-box helicase. Mol Cell Biol. 1999;19:6276–85.
39. Soto-Rifo R, Rubilar PS, Limousin T, de Breyne S, Décimo D, Ohlmann T. DEAD-box protein DDX3 associates with eIF4F to promote translation of selected mRNAs. EMBO J. 2012;31:3745–56.
40. Geissler R, Golbik RP, Behrens S-E. The DEAD-box helicase DDX3 supports the assembly of functional 80S ribosomes. Nucleic Acids Res. 2012;40:4998–5011.
41. Botlagunta M, Vesuna F, Mironchik Y, Raman A, Lisok A, Winnard P, et al. Oncogenic role of DDX3 in breast cancer biogenesis. Oncogene. 2008;27:3912–22.
42. Chen H-H, Yu H-I, Yang M-H, Tarn W-Y. DDX3 Activates CBC-eIF3-Mediated Translation of uORF-Containing Oncogenic mRNAs to promote metastasis in HNSCC. Cancer Res. 2018;78:4512–23.
43. Phung B, Cieśla M, Sanna A, Guzzi N, Beneventi G, Cao Thi Ngoc P, et al. The X-Linked DDX3X RNA helicase dictates translation reprogramming and metastasis in melanoma. Cell Rep. 2019;27:3573–86.e7.
44. Zhu Y, Hu Y, Tang C, Guan X, Zhang W. Platinum-based systematic therapy in triple-negative breast cancer. Biochim Biophys Acta Rev Cancer. 2022;1877:188678.
45. Gerratana L, Fanotto V, Pelizzari G, Agostinetto E, Puglisi F. Do platinum salts fit all triple negative breast cancers? Cancer Treat Rev. 2016;48:34–41.
46. Ding H, Zhang L, Wang Y, Liu S. Chinese Society of Clinical Oncology Breast Cancer (CSCO BC) guideline update: adjuvant therapy for triple negative breast cancer in 2022. Transl Breast Cancer Res. 2022;3:12.
47. da Costa AABA, Baiocchi G. Genomic profiling of platinum-resistant ovarian cancer: the road into druggable targets. Semin Cancer Biol. 2021;77:29–41.
48. Patch A-M, Christie EL, Etemadmoghadam D, Garsed DW, George J, Fereday S, et al. Whole-genome characterization of chemoresistant ovarian cancer. Nature. 2015;521:489–94.
49. Zhang D-Y, Sun Q-C, Zou X-J, Song Y, Li W-W, Guo Z-Q, et al. Long noncoding RNA UPK1A-AS1 indicates poor prognosis of hepatocellular carcinoma and promotes cell proliferation through interaction with EZH2. J Exp Clin Cancer Res. 2020;39:229.
50. Noel EE, Yeste-Velasco M, Mao X, Perry J, Kudahetti SC, Li NF, et al. The association of CCND1 overexpression and cisplatin resistance in testicular germ cell tumors and other cancers. Am J Pathol. 2010;176:2607–15.